Evaluating Thunderstorm Gust Fronts in New Mexico and Arizona

NICHOLAS T. LUCHETTI,[a] KATJA FRIEDRICH,[a] AND CHRISTOPHER E. RODELL[b]

[a] *Department of Atmospheric and Oceanic Sciences, University of Colorado Boulder, Boulder, Colorado*
[b] *Department of Earth, Ocean, and Atmospheric Sciences, University of British Columbia, Vancouver, British Columbia, Canada*

(Manuscript received 19 June 2020, in final form 28 September 2020)

ABSTRACT: Strong winds generated by thunderstorm gust fronts can cause sudden changes in fire behavior and threaten the safety of wildland firefighters. Wildfires in complex terrain are particularly vulnerable as gust fronts can be channeled and enhanced by local topography. Despite this, knowledge of gust front characteristics primarily stems from studies of well-organized thunderstorms in flatter areas such as the Great Plains, where the modification of gust fronts by topography is less likely. Here, we broaden the investigation of gust fronts in complex terrain by statistically comparing characteristics of gust fronts that are pushed uphill and propagate atop the Mogollon Rim in Arizona to those that propagate down into and along the Rio Grande Valley in New Mexico. Using operational WSR-88D data and in situ observations from Automated Surface Observing System (ASOS) stations, 122 gust fronts in these regions are assessed to quantify changes in temperature, wind, relative humidity, and propagation speed as they pass over the weather stations. Gust fronts that propagated down into and along the Rio Grande Valley in New Mexico were generally associated with faster propagation speeds, larger decreases in temperature, and larger increases in wind speeds compared to gust fronts that reached the crest of the Mogollon Rim in Arizona. Gust fronts atop the Mogollon Rim in Arizona behaved less in accordance with density current theory compared to those in the Rio Grande Valley in New Mexico. The potential reasons for these results, and their implications for our understanding of terrain influence on gust front characteristics, are discussed.

KEYWORDS: Complex terrain; Density currents; Gust fronts

1. Introduction

Rapid changes in wind direction and speed from passing thunderstorm gust fronts can threaten the safety of wildland firefighters by redirecting fire spread toward locations that were previously considered safe. In the past, studies of gust front characteristics have primarily focused on severe thunderstorms in flatter areas such as the U.S. Great Plains region (e.g., Charba 1974; Goff 1976; Engerer et al. 2008; Bryan and Parker 2010). However, little observational work has investigated the characteristics of gust fronts in complex terrain where thunderstorm outflow winds can be channeled and enhanced by local terrain features (Wakimoto et al. 1994; Goens and Andrews 1998; Sharples et al. 2017; Luchetti et al. 2020). Given that several dangerous fires occur in mountainous regions around the world each convective season, here we explore how gust fronts evolve and interact with local terrain in two complex terrain regions. Specifically, we statistically analyze the propagation and atmospheric characteristics (wind, temperature, moisture) of 122 gust fronts observed by in situ surface instruments in the complex terrain of New Mexico (NM) and Arizona (AZ) with the goal of exploring if variability in gust front characteristics can be linked to the underlying terrain.

Gust fronts are considered density currents with dense cold air propagating into an environment characterized by less dense and warmer air (e.g., Charba 1974; Sasaki and Baxter 1986; Friedrich et al. 2005). When thunderstorm gust fronts pass over a meteorological station, the station typically records an increase in wind speed, a rapid wind direction shift, a drop in temperature, and an increase in moisture content (Simpson 1969; Charba 1974; Goff 1976; Fujita 1981; Droegemeier and Wilhelmson 1987; Lompar et al. 2018; Luchetti et al. 2020). While temperature drop and moisture rise can act to diminish fire intensity (Hanley et al. 2013; Coen and Schroeder 2017; Coen et al. 2018), the ramp up of winds and directional shifts associated with gust front passage mostly overshadows these diminishing effects, and instead typically lead to rapid enhancement of fire intensity and spread. Several studies and accident reports emphasize gust front–induced wind direction change as the main catalyst for rapid fire intensification during accidents where individuals became entrapped and lost their lives (Surveys and Investigation Staff 1981; Haines 1988; Goens and Andrews 1998; Kern et al. 2004). Similarly, gust front–induced fire accidents and structural damage have occurred in areas of complex terrain where monitoring and tracking of thunderstorms can be more difficult (Karels and Dudley 2013; Johnson et al. 2014; Hardy and Comfort 2015; Paez et al. 2015). For example, during the destructive 2012 Colorado Waldo Canyon Fire multiple gust fronts rapidly shifted the direction of the fire spread toward a local neighborhood (Johnson et al. 2014). These wind shifts can also redirect fire spread toward topographic features favorable for fire growth such as canyons (Goens and Andrews 1998; Sharples et al. 2017). Considering the potential safety hazards associated with gust front–induced fire spread in mountainous areas, it is essential for the fire weather community to understand

Corresponding author: Nicholas Luchetti, nicholas.luchetti@colorado.edu

DOI: 10.1175/MWR-D-20-0204.1

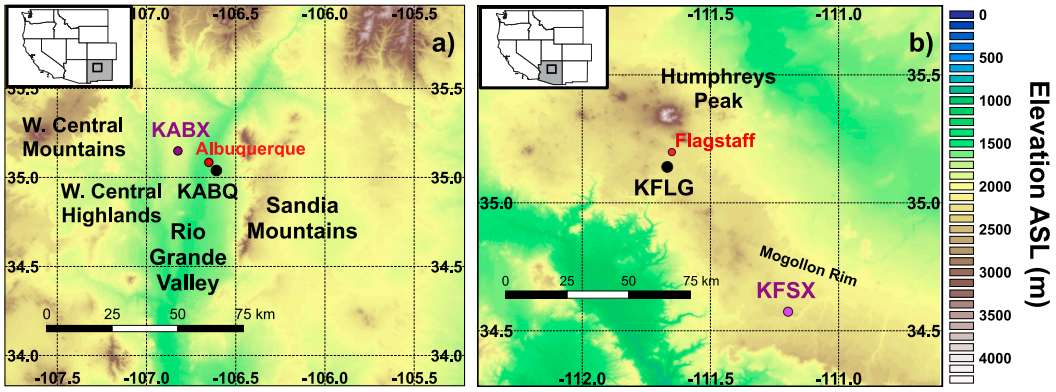

FIG. 1. Topographic maps showing the (a) New Mexico and (b) Arizona study regions. The location of the Albuquerque (KABQ) and Flagstaff (KFLG) ASOS stations are highlighted as the black dots. NWS Albuquerque (KABX) and the NWS Flagstaff (KFSX) NEXRAD radar sites are highlighted as the purple dots. Topographic features discussed in the text are highlighted.

how gust fronts evolve in these regions (Joint Fire Science Program 2017).

Our traditional understanding of gust front characteristics mostly stems from observational and numerical studies of gust fronts that initiate from severe thunderstorms such as mesoscale convective systems (MCSs) and supercell thunderstorms (e.g., Charba 1974; Goff 1976; Engerer et al. 2008; Bryan and Parker 2010), both of which tend to require flatter terrain to develop (Bunkers et al. 2006; Keighton et al. 2007; Parker and Ahijevych 2007; Schneider 2009; Ashley et al. 2019). While cases of MCS and supercell thunderstorms have been observed in areas of complex terrain in the past (LaPenta et al. 2005; Bosart et al. 2006; Schneider 2009), most thunderstorms that initiate across mountains typically remain as single or multicell thunderstorms until they can propagate into flatter regions (Cotton et al. 1983; McAnelly and Cotton 1986; Tucker and Crook 1999). This may be related to reduced temperatures, low-level moisture, and surface-based instability typically observed at higher elevations compared to lower elevations (Bunkers et al. 2006; Keighton et al. 2007; Schneider 2009). Despite this, single and multicell mountain thunderstorms can undoubtedly still produce gusty outflow boundaries with surface wind gusts strong enough to significantly alter fire behavior (Goens and Andrews 1998; Luchetti et al. 2020), and, therefore, need to be further evaluated.

Given the lack of focus on gust fronts in complex terrain regions throughout the literature, in this paper we broaden the investigation of gust front characteristics to those that evolve in the complex terrain of NM and AZ. The mountains of NM and AZ are ideal study regions as orographic thunderstorms frequently initiate during the North American Monsoon season between June and August (Adams and Comrie 1997). The chosen study areas also allow for the comparison of gust fronts that propagate across two differing terrain features commonly found in complex terrain regions: (i) up and over a ridgeline and (ii) down into a valley. To quantify gust front characteristics in these regions, we use the operational Weather Surveillance Radar-1988 Doppler (WSR-88D) radars in Albuquerque, NM, and Flagstaff, AZ, and Automated Surface Observing System (ASOS) weather stations.

The study is organized as follows: section 2 discusses the datasets and methods used including location, instrumentation, and local physiography for each of the two study regions. Results and comparisons between the study regions are presented in section 3. The potential role of topography on gust front characteristics is discussed in section 4. Conclusions and suggestions for future work are discussed in section 5.

2. Study sites, instrumentation, and analysis methods

a. Description of the study sites and the WSR-88Ds

To study gust front characteristics in complex terrain, we choose two study sites near Albuquerque, NM, and Flagstaff, AZ (Fig. 1). These study sites are chosen based on the following criteria. Each site needs to (i) be located in complex terrain, (ii) have a convective season, (iii) experience wildfires during the convective season, (iv) be within 80 km range of an operational WSR-88D, and (v) have at least one ASOS station within the 80 km radar range.

The two WSR-88Ds used to identify and track gust fronts are the Albuquerque, NM, radar (referred to as KABX hereafter; Fig. 1a) and the Flagstaff, AZ, radar (referred to as KFSX hereafter; Fig. 1b). KABX is located 20 km northwest of Albuquerque at 1.8 km MSL in the Rio Grande Valley between the NM West Central Highlands and Mountains to the west and the Sandia Mountains to the east (Fig. 1a). Thunderstorms that impact the Albuquerque region often originate from the West Central Mountains farther west or the Sandia Mountains to the east. Within the 80 km range, the KABX radar beam at the lowest elevation angle of 0.47° experiences no beam blockage to the southeast and throughout the surrounding Rio Grande Valley at the radar (Shipley et al. 2009). However, along the crest and to the east of the north–south-oriented Sandia Mountains, the KABX radar beam experiences 50%–100% beam blockage. Additionally, the KABX radar beam experiences 20%–50% beam blockage toward the west and over the West Central Highlands and Mountains

region. Therefore, identifying and tracking gust fronts east of the Sandia Mountains and over the West Central Highlands region is more challenging compared to those that occur in the Rio Grande Valley.

KFSX is located about 79 km southeast of Flagstaff at 2.3 km MSL atop the Mogollon Rim (Fig. 1b), which favors convection initiation in the afternoon during the convective season (Adams and Comrie 1997; Goens and Andrews 1998). Within the 80 km range, the KFSX radar beam at the lowest radar elevation angle of 0.47° experiences roughly 20%–30% beam blockage to the northwest toward Humphreys Peak (Fig. 1b), and directly south to the edge of Mogollon Rim (Shipley et al. 2009). However, the KFSX radar beam experiences no beam blockage along the remainder of the Mogollon Rim to the east and west. Therefore, from a beam blockage perspective, identifying and tracking gust fronts on the east and west edge of the Mogollon Rim is less challenging than for those gust fronts that develop to the north near Humphreys Peak. Since the KFSX radar is located on top of the Mogollon Rim, lower terrain to the east and west is ~1–1.5 km below the radar. Gust fronts originating in the lower terrain might not be captured by the lowest 0.47° radar scan until they move up to the Mogollon Rim.

b. *Description of automated surface observing system instrumentation*

Surface data from the ASOS weather stations are used to assess the change in horizontal wind speed and direction, temperature, and relative humidity during gust front passage. ASOS stations provide high-resolution measurements of basic weather elements that undergo multiple levels of quality control (Nadolski 1998). Wind speed and direction is measured at 10 m above ground level (AGL) using a sonic anemometer every 1 s from which a 3 s running mean is computed producing a "3 s peak" (NWS 2008). A running 2-min average is then computed across 24 discrete 5 s samples. The value of the 2-min-averaged peak wind speed consists of the "3 s peak" from the 5 s sample that contains the highest "3 s peak" wind speed (NWS 2008). Wind gusts are also measured and updated every 3 s. The accuracy for wind direction is ±3° for winds greater than 2.5 m s^{-1}, and the accuracy for wind speed is ±1 m s^{-1}. The ambient dry-bulb and dewpoint temperatures are measured using a HO-83 hygrothermometer every 10 s and averaged to 1-min intervals. The 5-min averages of the 1-min-averaged intervals are then reported every 1 min. Accuracies for temperature and dewpoint temperature measurements are within ±1° and ±3°C, respectively. Here, we utilize 1-min averages of wind, temperature, and relative humidity to evaluate gust front events in these study regions.

The New Mexico ASOS station (KABQ) is located at 1.6 km MSL just downslope of the Sandia Mountains in the Rio Grande Valley about 23 km southeast of the operational radar KABX (Fig. 1a). Considering the height difference between the radar and the ASOS station, the center of the lowest radar beam at 0.47° elevation is about 0.2 km above the KABQ station.

The Arizona ASOS station (KFLG) is located at 2.1 km MSL on the Mogollon Rim just south of Humphreys Peak (Fig. 1b) and about 76 km northwest of the operational radar KFSX. Considering the height difference between the radar and the ASOS station, the center of the lowest radar beam at 0.47° elevation is about 0.9 km above the KFLG station.

c. *Gust front detection and tracking method and categorizing*

To quantify changes in wind, temperature, and moisture associated with a gust front, we first need to identify the times when a gust front passes over one of the ASOS stations. To do that, we identify days during the 2010–18 monsoonal seasons (June–August) when thunderstorms develop in close proximity to the ASOS stations using Level II radar reflectivity at the lowest level at 0.47° elevation every 5 min from the operational WSR-88Ds. From those days, we isolate the days where lines of reflectivities of 5–25 dBZ (also radar fine lines) propagate away from a parent thunderstorm and pass through the ASOS station (Fig. 2). Identifying thunderstorm gust fronts via the radar fine lines is a widely accepted method (Wilson and Schreiber 1986; Koch and Ray 1997; Luchetti et al. 2020). Tracking of radar fine lines is used to determine (i) the time when gust fronts pass over the ASOS stations and (ii) gust front propagation speed and direction between the time of first detection and passage through the station (Fig. 2). Gust front propagation speed is determined by calculating the displacement of the radar-detected fine lines over time as they approach and pass over the ASOS stations. Since radar fine lines tend to morph into irregular shapes, we account for this by determining an approximately 10 km mean positional swath across the leading edge of the boundary as it moves over the ASOS stations. The swath displacement is then tracked backward to calculate the mean propagation speed between the time the fine line is first detected and the time it passes over the ASOS stations. Level II radar reflectivity is also used to categorize parent thunderstorms as single-cell, multicell, quasi-linear, or supercell thunderstorms following Smith et al. (2012).

d. *Magnitude change calculation*

Once we determine the time when each radar-indicated gust front passes over the ASOS stations, we then quantify the change in wind speed and direction, temperature, and relative humidity during that time (referred to as the magnitude change and described in more detail in Luchetti et al. 2020). In situ 1-min ASOS data are analyzed 30 min prior to and 30 min after the radar-indicated gust front passage time (Fig. 3). During this timeframe we identify the time when the largest gradient in each atmospheric variable occurs (yellow box in Fig. 3, referred to as the Gust Front Passage Period or GPP; Luchetti et al. 2020). We then quantify the magnitude change in each atmospheric variable by taking the difference between the 5-min mean of the variable prior to and after the GPP (green boxes in Fig. 3). The magnitude change is analyzed for each atmospheric variable across all gust front events in each of the two study areas.

e. *Gust front area clustering*

To determine the role of the underlying terrain on gust front characteristics, we first group radar fine lines based on where

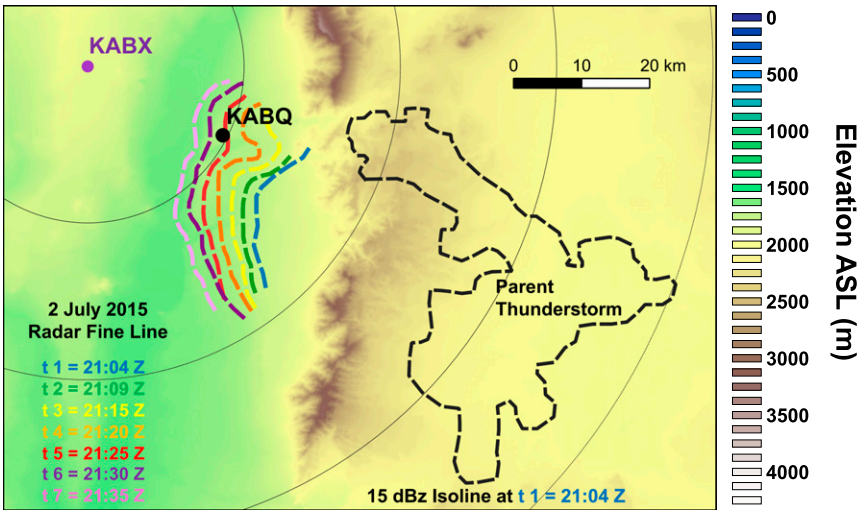

FIG. 2. Topographic map with the time series of the position of a radar fine line that passed over the KABQ ASOS site (black dot) on 2 Jul 2015 observed by the KABX operational radar (purple dot) at Albuquerque, New Mexico. Radar reflectivity at 0.47° radar elevation angle approximately every 5 min is used to track the movement of the 5–25 dBZ radar fine line from the time it first appears (t1) until it passes the KABQ ASOS station (t7). The 15 dBZ isoline of the parent thunderstorm at t1 is outlined (dashed black line). KABX radar range rings at 25 km intervals are displayed as thin black lines with the radar site at the center.

they are first observed and from which direction they approach the ASOS station. To do this, we digitize the entire extent of the radar fine line from its first detection till it passes over the ASOS station using Level II radar reflectivity and ArcGIS (ESRI 2011). In a next step, we group each gust front based on the location where the gust front is first detected with respect to the topography around the ASOS stations and from which direction the gust front approaches the ASOS station. The NM study region is divided into three main groups with gust fronts (Fig. 4) that are first (i) detected and continued to propagate through the Rio Grande Valley, (ii) detected over the Sandia Foothills and Mountains and continued to propagate downhill into the Rio Grande Valley, and (iii) detected over the West Central Highlands and continued to propagate into the Rio Grande Valley (Fig. 4; Table 1). Gust fronts in the Rio Grande Valley are further subdivided depending on where they are first detected north, south, or west of the ASOS station. Gust fronts from the Sandia Foothills and Mountains are subdivide into gust fronts that are first observed over the Foothills (Sandia Foothills) and those detected over the mountains (Sandia Mountains; Fig. 4). The gust front detected on 2 July 2015 shown in Fig. 2 would be placed into the Sandia Foothills group as it was first detected along the foothills approaching the station from the southeast.

In the AZ study region, gust fronts are grouped into those that are first detected on top of the Mogollon Rim (i) east, (ii) north, or (iii) south of the ASOS station (Fig. 6; Table 2). Note that as the radar is located on top of the Rim, gust fronts originating in the lower terrain about ~1–1.5 km lower than the radar height might not be captured by the lowest radar scan at 0.47° until they move up to the Rim.

Note that the gust front grouping in each region is based on the location of when and where the fine lines are first detected by the operational radars, but do not necessarily represent the location and timing of when the gust fronts actually initiate. In NM, this is especially true east of the Sandia Mountains, where the radar beam blockage is high (50%–100%) relative to the other NM areas. Similar challenges exist for detecting the initiation of gust fronts that propagate down from Humphreys Peak and up the sidewalls of the Mogollon Rim in AZ where the radar scan height is ~1–1.5 km AGL. Shallow gust fronts in these regions may not be detectable until they migrate within a closer range of the radars or into areas with less beam

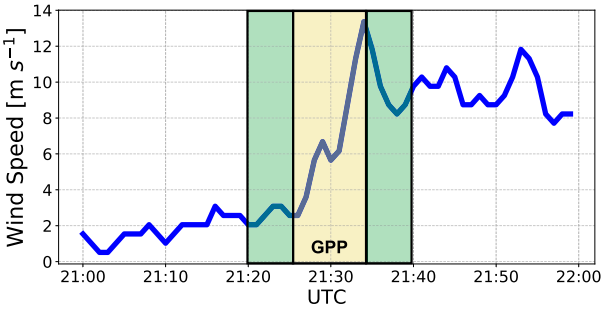

FIG. 3. Temporal evolution of horizontal wind speed (m s^{-1}) during a gust front passage on 2 Jul 2015 over the KABQ ASOS site. White area indicates the time 30 min prior to and 30 min after the radar-derived gust front passage time. The yellow-highlighted box represents the gust front passage period (GPP). The green-highlighted areas represent the 5-min intervals where the variable is averaged in order to calculate the difference in the variable prior to and after the GPP.

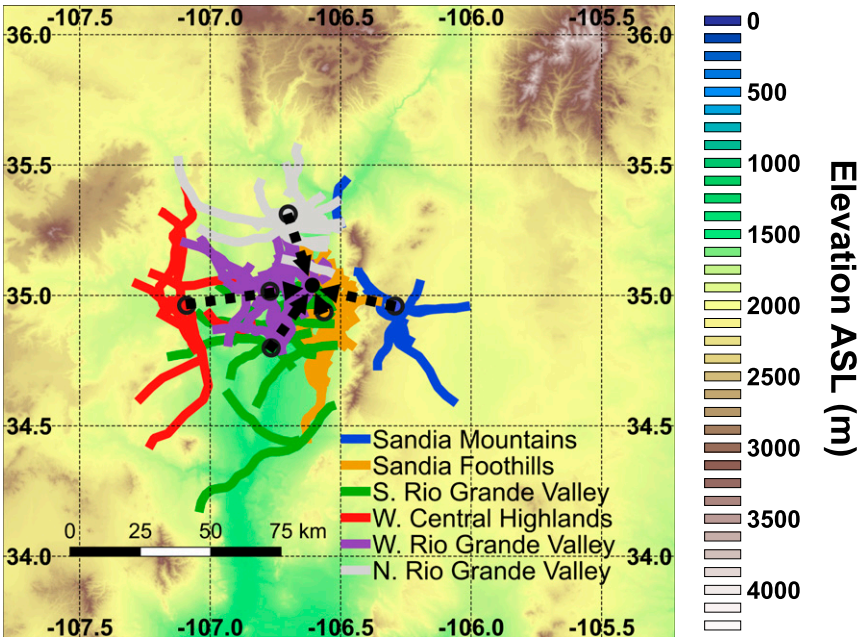

FIG. 4. Topographic map with radar fine lines for the 79 New Mexico gust fronts at the moment they first appear on the KABX operational radar at Albuquerque, New Mexico. Gust fronts are grouped into six groups depending the location of first detection and the direction they propagate toward the KABQ New Mexico ASOS station (black dot). The open colored circles represent the centroid of each gust front group. The black dashed arrows represent the path between the centroid and the ASOS station used to calculate the approximate terrain profile.

blockage. Despite this, grouping the gust fronts based on when and where the radars first detect them still provides intercomparisons of gust fronts that encounter differing terrain features as they approach the ASOS stations.

f. Terrain profiles

After grouping the gust fronts, we then calculate the initial detection centroid of all digitized gust front fine lines in each group (open circle in Figs. 4 and 6) and the terrain profile between the centroid and the ASOS station. By doing so, we can compare how differences in the variability of terrain for each group might influence gust front propagation and its atmospheric characteristics. To calculate the initial detection centroid for each group, we first calculate the center point of each digitized radar fine line. The initial detection centroid is then found by calculating the weighted mean center of all radar fine line center points. The terrain profile consists of the height change between the initial detection centroid and the ASOS station and the mean terrain slope over the entire profile. The latter indicates if the gust fronts predominantly propagates downhill, experiencing adiabatic warming, or uphill, experiencing orographic lift and cooling.

Once terrain profiles for each gust front group are calculated, we statistically compare the mean propagation speed and

TABLE 1. Event overview for the 79 gust fronts observed between 2010 and 2018 passing over the New Mexico ASOS station. Gust fronts are grouped into six areas depending on the location of first detection and the direction from which they approach the ASOS station. Number of gust fronts (N), the range of directions from which gust fronts propagate (°), the fraction of events that occurred in June, July, and August, and the fractional breakdown of parent thunderstorm (PTS) type are listed.

Gust front area	N	Propagation direction range (°)	Fraction of events in Jun (%)	Fraction of events in Jul (%)	Fraction of events in Aug (%)	Fraction of single-cell PTS (%)	Fraction of multicell PTS (%)
Sandia Mountains	5	60–120	25	75	0	60	40
Sandia Foothills	30	60–150	1	76	13	77	23
South Rio Grande valley	10	135–195	20	50	30	40	60
West Central Highlands	7	225–315	14	14	72	50	50
West Rio Grande valley	16	225–315	0	63	37	50	50
North Rio Grande valley	11	315–45	36	27	37	45	55

TABLE 2. As in Table 1, but the event overview for the 43 gust fronts passing over the Arizona ASOS station.

Gust front area	*N*	Propagation direction range (°)	Fraction of events in Jun (%)	Fraction of events in Jul (%)	Fraction of events in Aug (%)	Fraction of single-cell PTS (%)	Fraction of multicell PTS (%)
East Mogollon Rim	26	15–135	0	77	23	38	62
North Mogollon Rim	14	300–360	12	65	23	71	29
South Mogollon Rim	3	180–225	67	33	0	67	33

atmospheric characteristics within each study region and among the two study regions. We then explore if any differences in atmospheric characteristics can be attributed to the differing terrain profiles. We acknowledge that by using the centroids and mean terrain profiles not all gust fronts within each group follow the exact same terrain path to the ASOS station. To address that we also conduct a sensitivity study where we use the exact terrain profile between the center point of each initially detected radar fine line and the ASOS station. However, we expect the deviation from the centroid terrain profile to be minimal for each gust front profile, and therefore suspect that the centroid terrain profiles will be sufficient for facilitating comparisons among groups.

3. Results

a. Events overview and regional comparison

During the 2010–18 monsoon seasons (June–August) 79 thunderstorm gust fronts are identified as radar fine lines that pass through the KABQ station in Albuquerque. Gust fronts are first observed either over the terrain to the east and west of the station (53%) or within the Rio Grande Valley (47%). Gust fronts propagate from the West Central Highlands approaching the ASOS station from the west (9% of the cases) or the Sandia Foothills (38%) and Mountains (6%) east of the ASOS station (Table 1; Fig. 4) propagating downslope into the Rio Grande Valley with mean slopes between −3° and −22° (Fig. 5). Gust fronts also propagate downslope from the northern (14%) or western (20%) Rio Grande Valley with mean slopes of −11° and −14°, respectively. In total, 13% of the NM gust fronts are first observed in the southern Rio Grande Valley (Table 1; Fig. 4) and approach the station from the south and uphill with a mean slope of +6° (Fig. 5).

The largest number of gust fronts is observed in either July or August (Table 1). Note that, the number of gust fronts in the North Rio Grande Valley is more evenly spread across the 3 months compared to the West Central Highlands, Sandia Foothills, and Sandia Mountains. The gust fronts in this study develop from either single or multicell thunderstorms, with a relatively even spread between the two thunderstorm types for most of the areas (Table 1). Note that supercell parent thunderstorms and squall lines are not observed during this time period in this area. The dominance of single and multicell thunderstorms and lack of supercell thunderstorms has also been observed in other studies of thunderstorms in complex terrain (Cotton et al. 1983; McAnelly and Cotton 1986; Tucker and Crook 1999; Luchetti et al. 2020).

In AZ, a total of 43 gust fronts are identified to pass through the KFLG ASOS station during the 2010–18 monsoon seasons (June–August). Gust fronts are first observed on top of the Mogollon Rim east of the ASOS station traveling westward (60% of the cases), north of the station traveling southward (33%), and south of the ASOS station traveling northward (7%; Table 2; Fig. 6). East and South Mogollon Rim gust fronts propagate mainly uphill (mean slopes of 20° and 27°), while those from the North Mogollon Rim propagate mainly downhill with a mean slope of −24° (Fig. 7). Most of the gust fronts in the AZ study region also predominantly occur in the wetter monsoon months (July–August; Table 2). Similar to the NM gust fronts, all AZ gust fronts in this study develop from single or multicell thunderstorms (Table 2).

The NM and AZ study regions are similar in that they both reside in a predominantly dry climate and thunderstorms and precipitation are most frequent during the North American moonson period (Adams and Comrie 1997). As outlined above, the two study regions differ in the dominant terrain feature present in each area with NM gust fronts predominantly propagating downhill into a valley (Fig. 4) and AZ gust fronts being either pushed uphill or propagate on top of a major ridgeline (Fig. 6). For the remaining analysis we will focus on exploring statistical differences between gust fronts that propagate down into and along a valley (NM) and those that are pushed up to and propagate on a ridgeline (AZ), as

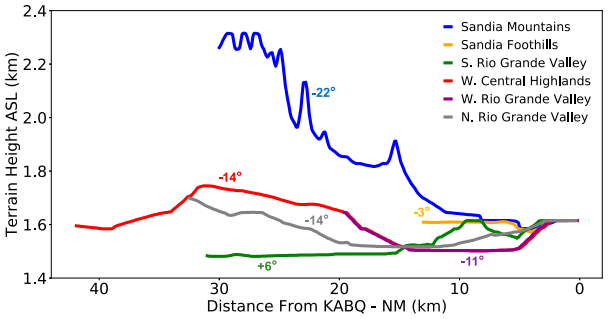

FIG. 5. Terrain height above mean sea level (MSL) (km) along each New Mexico gust front area's propagation path to the KABQ ASOS station located at 0 km. Solid lines represent the terrain profile calculated from the mean centroid location of the detected radar fine lines for each gust front area to the KABQ ASOS station. Terrain profiles are derived using data from the 1/3 arc-second U.S. Geological Survey (USGS) National Elevation Dataset (NED). The mean directional slope along each group's path is annotated as either a minus sign (−) for downhill or a plus sign (+) for uphill.

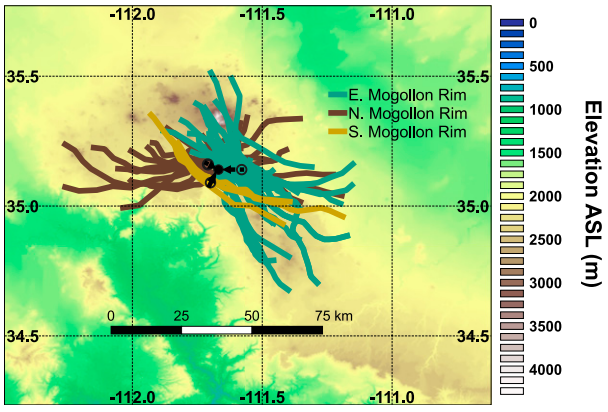

FIG. 6. As Fig. 4, but for the 43 Arizona gust fronts observed by the KFSX operational radar at Flagstaff, Arizona. Gust fronts are grouped into three groups depending the location of first detection and the direction they propagate toward the KFLG Arizona ASOS station (black dot).

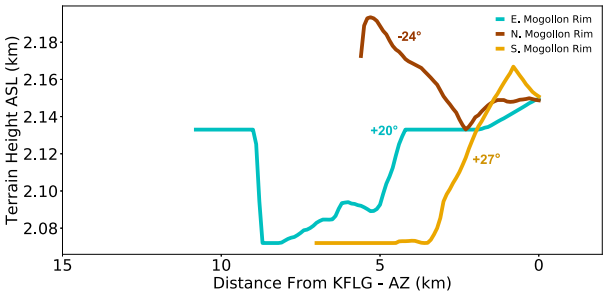

FIG. 7. Terrain height above mean sea level (MSL) (km) along each Arizona gust front area's propagation path to the KFLG ASOS station at 0 km. Solid lines represent the terrain profile calculated from the mean centroid location of the detected radar fine lines for each gust front area to the KFLG ASOS station. Terrain profiles are derived using data from the 1/3 arc-second U.S. Geological Survey (USGS) National Elevation Dataset (NED). The mean directional slope along each area's path is also annotated as either a minus sign (−) for downhill or a plus sign (+) for uphill.

well as analyze any localized terrain effects among the categorized gust front areas in both regions.

b. Propagation speed and magnitude changes

1) GUST FRONT PROPAGATION SPEED

When comparing the median propagation speed ($\widetilde{\text{pspd}}$) at the time of passage over the ASOS stations, NM gust fronts are faster with $\widetilde{\text{pspd}}$ ranging from 7.9 to 11.9 m s^{-1} (Fig. 8a), compared to AZ area gust fronts with $\widetilde{\text{pspd}}$ ranging from 4.1 to 7.2 m s^{-1} (Fig. 8b). Additionally, the mean propagation speed ($\overline{\text{pspd}}$) calculated across all 79 NM gust fronts is on average faster at 8.6 m s^{-1} compared to 5.2 m s^{-1} across the 43 AZ gust fronts (statistically significantly different at $p < 0.05$ using a two-sided Student's t test) (Fig. 8). In general, the gust fronts in this study that propagate downhill into and along the Rio Grande Valley in NM are faster compared to the gust fronts that are pushed up to the crest of the Mogollon Rim in AZ. These results are likely related to acceleration by cold air density currents, which is typically observed in laboratory experiments of density currents traveling downslope (e.g., Dai et al. 2012; Dai and Huang 2016; He et al. 2017).

We also analyze the influence of the prefrontal ambient wind on each gust front, which can act to slow down (headwind) or speed up (tailwind) propagating gust fronts (Simpson and Britter 1980; Jorgensen et al. 2003). Fitting the observed propagation speed to the prefrontal ambient wind through linear regression (Fig. 9a), we find that faster gust fronts in the Rio Grande Valley in NM often do not have stronger tailwinds with a coefficient of determination of $R^2 = 0.07$ and correlation of $r = 0.26$ (not statistically significant at $p < 0.05$ using a two-sided t test with confidence intervals based on the Fisher transformation). This suggests that there is no linear relationship between the prefrontal ambient wind and the gust front propagation speed in the NM cases discussed here. Atop the Mogollon Rim in AZ, however, this linear relationship is slightly stronger with $R^2 = 0.32$ and $r = 0.57$ (statistically significant at $p < 0.05$ using a two-sided t test with confidence intervals based on the Fisher transformation), suggesting that faster (slower) AZ gust fronts often do have stronger tailwinds (headwinds) (Fig. 9b). Note that both Breusch–Pagan and White tests are performed as the data in Fig. 9b visually appears to be heteroscedastic. Both tests resulted in high p values, concluding that the data are not heteroscedastic and, therefore,

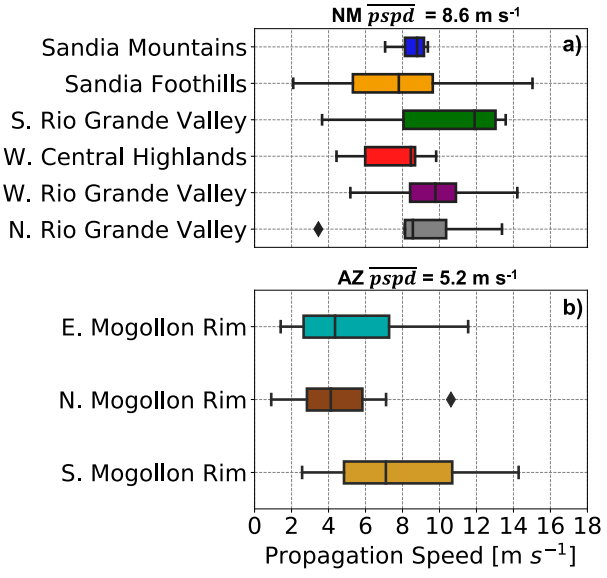

FIG. 8. Box-and-whiskers plots of radar-derived gust front propagation speeds (m s^{-1}) for gust front groups observed in (a) New Mexico and (b) Arizona. The mean propagation speed across all 79 NM and 43 AZ gust fronts is listed at the top of (a) and (b), respectively. The filled boxes represent the interquartile range for each individual gust front area in both study regions. The whiskers extend to data points that fall within 1.5 times the interquartile range of the lower and upper quantiles. Outliers that fall beyond this range are independently represented by diamond symbols. Colors correspond to each individual gust front area shown in Figs. 4 and 6.

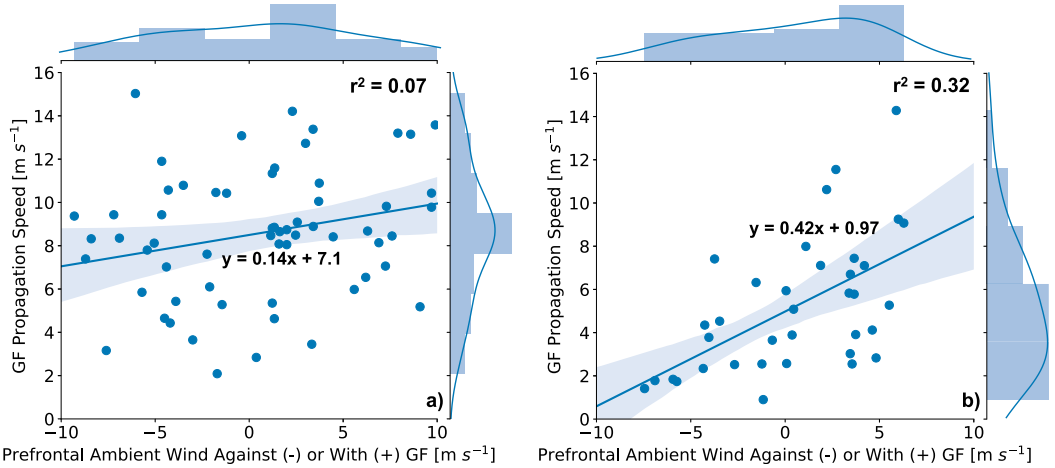

FIG. 9. Scatterplot of radar-derived propagation speed ($m\,s^{-1}$) as a function of the prefrontal ambient wind component ($m\,s^{-1}$) for gust fronts in (a) New Mexico and (b) Arizona. The prefrontal cross-front ambient wind is derived by wind anemometers deployed at the ASOS stations. Linear regression fit is plotted as the solid blue line with coefficient of determination (r^2) shown in the top right. The blue shaded region surrounding the regressed fit is the 95% confidence intervals of the regression. The fitted distribution for each axis is displayed as histograms.

linear regression is not violated. However, the gust front propagation speed in Fig. 9b does appear to increase in variability as the magnitude of the prefrontal tailwind increases. This may suggest that if the tailwind is too strong, it may suppress the gust front as opposed to accelerate it in some cases. This is often reported in studies of sea breeze (also a density current) interactions with onshore ambient tailwinds (e.g., Arritt 1993; Gilliam et al. 2004). Regardless, the gust fronts in this study that are pushed up to the crest of the Mogollon Rim in AZ are more likely to be influenced by the magnitude and direction of the prefrontal ambient wind compared to those gust fronts propagating down into and along the Rio Grande Valley in NM.

2) GUST FRONT TEMPERATURE, RELATIVE HUMIDITY, WIND SPEED, AND DIRECTION

The median temperature decrease ($\Delta\tilde{T}$) during passage for NM gust fronts ranges from 0.4° to 2.8°C (Fig. 10a), compared to AZ gust fronts with $1.3° < \Delta\tilde{T} < 2.8°C$ (Fig. 10e). Additionally, when comparing the mean temperature difference ($\Delta\overline{T}$) across all gust front events in both regions, we find that the $\Delta\overline{T}$ decrease is on average larger for the 79 NM gust fronts ($\Delta\overline{T} = -2.2°C$) when compared to the 43 AZ gust fronts where $\Delta\overline{T} = -1.5°C$ (Fig. 10). The difference is statistically significant at $p < 0.05$ using a two-sided Student's t test. Therefore, the gust fronts in this study that propagate down into and along the Rio Grande Valley in NM experience larger decreases in temperature compared to the gust fronts that are pushed up to the crest of the Mogollon Rim in AZ. Again, these findings are consistent with density current experiments, which show that for currents traveling upslope, the associated cold air driving the current tends to thin out with increasing upslope angles (Marleau et al. 2014; Lombardi et al. 2015; De Falco et al. 2020).

The median change in relative humidity ($\Delta\widetilde{RH}$) is smaller across the NM area gust fronts ranging from −0.01% to 6.7% (Fig. 10b), compared to the AZ gust fronts with $3.2 < \Delta\widetilde{RH} < 10.4\%$ (Fig. 10f). The mean change in relative humidity ($\Delta\overline{RH}$) across all 43 AZ gust fronts is also higher ($\Delta\overline{RH} = 5.8\%$) compared to the 79 NM gust fronts ($\Delta\overline{RH} = 3.5\%$) with a statistically significant difference at $p < 0.05$ using a two-sided Student's t test (Fig. 10). Gust fronts in this study that propagate atop the Mogollon Rim in AZ, therefore, experience larger increases in RH compared to those that propagate down into and along the Rio Grande Valley in NM. An analysis of the dewpoint temperature change (ΔT_d) reveals that the AZ gust fronts are associated with larger changes in absolute moisture ($\Delta\overline{T}_d = 1.8°C$) during gust front passage compared to NM gust fronts ($\Delta\overline{T}_d = 0.8°C$) (statistically significantly different at $p < 0.05$ using a two-sided Student's t test; not shown). Thus, relative to the prefrontal ambient air, gust fronts that propagate down into Rio Grande Valley in NM are cooler, but also drier compared to those atop the Mogollon Rim in AZ, which explains the smaller changes in RH observed in NM.

As the gust fronts pass through the ASOS stations, the median increase in horizontal wind speed ($\Delta\widetilde{wsp}$) is larger across the NM gust fronts ranging from 5.2 to $8.7\,m\,s^{-1}$ (Fig. 10c), compared to the AZ gust fronts with $2.9 < \Delta\widetilde{wsp} < 4.8\,m\,s^{-1}$ (Fig. 10g). Furthermore, the mean increase in wind speed ($\Delta\overline{wsp}$) across all 79 NM gust fronts is larger ($\Delta\overline{wsp} = 7.5\,m\,s^{-1}$) compared to the 43 AZ gust fronts ($\Delta\overline{wsp} = 3.5\,m\,s^{-1}$). The difference between $\Delta\overline{wsp}$ is statistically significant at $p < 0.05$ using a two-sided Student's t test (Fig. 10). Thus, the gust fronts in this study that propagated downhill into and along the Rio Grande Valley in NM generally produced larger increases in wind speed compared to those that are pushed up to and propagate atop the Mogollon Rim in AZ. These results agree with density current theory that suggests that the larger the temperature difference between the cold air of the density current and the warmer environmental air (true for NM gust fronts in this study), the stronger the difference in wind speeds

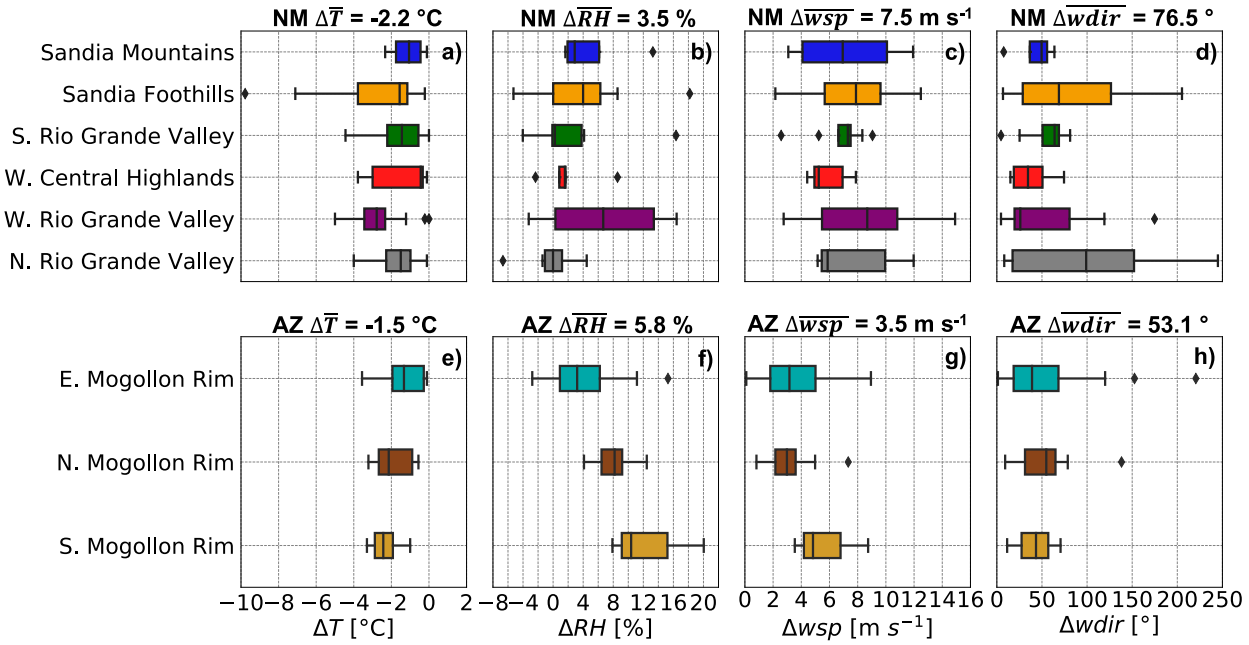

FIG. 10. As in Fig. 8, but for the (a),(e) magnitude change in temperature (°C); (b),(f) the magnitude change in relative humidity (%); (c),(g) the magnitude change in wind speed ($m\,s^{-1}$); and (d),(h) the magnitude change in wind direction (°). The mean value for each variable across the 79 NM gust fronts is listed atop (a)–(d), and the mean value for each variable across the 43 AZ gust fronts is listed atop (e)–(h).

across the different air masses (Benjamin 1968; Simpson and Britter 1980; Jorgensen et al. 2003).

After passing over the ASOS stations, the median absolute magnitude change in wind direction ($\Delta\widetilde{\text{wdir}}$) is larger across the NM gust fronts ranging between 26.2° and 99.3° (Fig. 10d) compared to the AZ gust fronts with $39.2° < \Delta\widetilde{\text{wdir}} < 54.8°$ (Fig. 10h). Using a two-sided Student's t test, the mean wind direction change across the 79 NM gust fronts ($\Delta\overline{\text{wdir}} = 76.5°$) is found to be statistically significantly larger at $p < 0.05$ when compared to $\Delta\overline{\text{wdir}}$ across the 43 AZ gust fronts ($\Delta\overline{\text{wdir}} = 53.1°$). Therefore, gust fronts that propagated downhill into the Rio Grande Valley in NM on average produce larger $\Delta\overline{\text{wdir}}$ compared to those that propagated atop the Mogollon Rim in AZ.

3) Relationship between magitude change in temperature and wind speed

In both terrain regions, the magnitude decrease in temperature is often accompanied by a magnitude increase in horizontal wind speed (Fig. 11). However, this relationship is considerably stronger for gust fronts in the Rio Grande Valley in NM with a correlation of $r = 0.57$ and $R^2 = 0.33$ (statistically significant at $p < 0.05$ using a two-sided t test with confidence intervals based on the Fisher transformation) (Fig. 11a), compared to those atop the Mogollon Rim in AZ ($r = 0.28$; $R^2 = 0.08$; not statistically significant at $p < 0.05$ using a two-sided t test with confidence intervals based on the Fisher transformation) (Fig. 11b). Therefore, the gust fronts in this study that propagate downhill into and along the Rio Grande Valley in NM tend to behave more consistently in accordance with density current theory. Gust fronts atop the Mogollon Rim in AZ, however, do not behave like density currents considering the weak relationship ($r = 0.28$; $R^2 = 0.08$) between the magnitude decrease in temperature and the magnitude increase in horizontal wind speed observed here (Fig. 11b).

While the NM gust fronts discussed thus far are associated with expected decreases in temperature during passage over the KABQ ASOS station, we did observe 15 additional gust fronts (not included in the analysis pertaining to the 79 NM cases discussed above) that actually induce an increase in temperature during passage (not shown). The mean propagation speed ($\overline{\text{pspd}}$) across these 15 gust fronts at time of passage is $8.2\,m\,s^{-1}$, with a mean increase in wind speed ($\Delta\overline{\text{wsp}}$) of $5.1\,m\,s^{-1}$. These 15 gust fronts are visible on radar as fine lines propagating at speeds similar to the 79 NM gust fronts ($\overline{\text{pspd}} = 8.6\,m\,s^{-1}$) associated with decreases in temperature (Fig. 8a). Perhaps, the cold air driving these 15 gust fronts may be elevated above the surface and, thus, the boundary is only detectable as a radar fine line and not by the ASOS station itself. An alternative hypothesis, however, is perhaps these 15 gust fronts are simply associated with very little precipitation, resulting in weak gust fronts that induce downslope warming observed by the ASOS station.

4. Discussion—Role of topography

Terrain profiles for each study region are calculated to quantify the potential influence of adiabatic heating and cooling on gust front characteristics (see section 2f, Figs. 5 and 7).

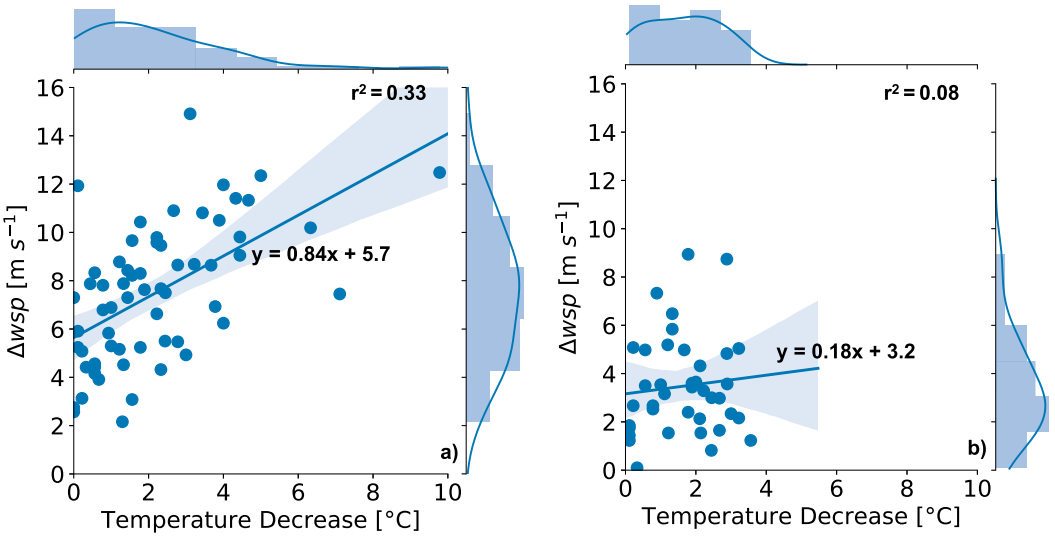

FIG. 11. As in Fig. 9, but comparison of the magnitude change in wind speed ($m\,s^{-1}$) as a function of the decrease in temperature (°C) measured by the ASOS stations in (a) New Mexico and (b) Arizona.

For NM gust fronts that propagate downhill, smaller $\Delta\tilde{T}$ and $\Delta\widetilde{wsp}$ are observed for gust fronts from areas experiencing steeper terrain downslopes (−14° to −22°) (e.g., Sandia Mountains, West Central Highlands, North Rio Grande Valley; Figs. 10a,c), when compared to areas experiencing shallower terrain downslopes (−3° to −11°) (e.g., Sandia Foothills and West Rio Grande Valley; Figs. 10a,c). Statistically, a positive, albeit weak relationship between the magnitude decrease in temperature and the mean terrain slope calculated for each individual NM gust front is observed ($r = 0.24$; $R^2 = 0.06$, statistically significant at $p < 0.05$ using a two-sided t test with confidence intervals based on the Fisher transformation) (Fig. 12a). This suggests that larger magnitude decreases in temperature are weakly associated with less negative mean terrain slopes. Furthermore, a positive relationship between the magnitude change in wind speed and the mean terrain slope for each individual NM gust front is observed ($r = 0.36$; $R^2 = 0.13$, statistically significant at $p < 0.05$ using a two-sided t test with confidence intervals based on the Fisher transformation) (Fig. 12b). This suggests that larger increases in wind speed are also weakly associated with less negative mean terrain slopes for the NM cases studied here. Therefore, perhaps subtle differences in gust front strength can be partially attributed to the degree of downslope adiabatic warming potential for gust fronts that propagate down or within valley slopes.

In AZ, there is no discernable relationship between upslope or downslope adiabatic processes and gust front strength. For example, $\Delta\tilde{T}$ for gust fronts from the North Mogollon Rim is actually larger ($\Delta\tilde{T} = -2.1$°C) than for gust fronts from the East Mogollon Rim with $\Delta\tilde{T} = -1.3$°C (Fig. 10e), despite a strong mean terrain downslope (−24°) profile from the north side of the rim (Fig. 7). Similarly, $\Delta\widetilde{wsp}$ is essentially identical ($\Delta\widetilde{wsp} = 2.9\,m\,s^{-1}$; $\Delta\widetilde{wsp} = 3.0\,m\,s^{-1}$) when comparing these two areas (Fig. 10g). For gust fronts from the South Mogollon Rim, whether upslope adiabatic cooling contributes to the larger median temperature decrease ($\Delta\tilde{T} = -2.8$°C) (Fig. 10e) and larger median increase in wind speed ($\Delta\widetilde{wsp} = 4.8\,m\,s^{-1}$) (Fig. 10g) is difficult to discern with only three gust front cases. Statistically, the correlation between the magnitude decrease in temperature and the mean terrain slope calculated for each individual AZ gust front is very weak ($r = 0.03$; $R^2 = 0.001$, not statistically significant at $p < 0.05$ using a two-sided t test with confidence intervals based on the Fisher transformation) (Fig. 13a). This further suggests no connection between the degree of downslope warming or upslope cooling potential and the magnitude decrease in temperature associated with the AZ gust fronts analyzed here. A weakly positive relationship between the magnitude change in wind speed and the mean terrain slope for each individual AZ gust front is observed ($r = 0.35$; $R^2 = 0.11$) (Fig. 13b). However, this relationship is not statistically significant at $p < 0.05$ when using a two-sided t test with confidence intervals based on the Fisher transformation. Therefore, given these weak, nonstatistically significant relationships, the degree of downslope adiabatic warming or upslope cooling potential does not influence gust front strength for the AZ cases studied here.

While localized adiabatic influence on the gust fronts in this study is hard to discern, comparisons of gust fronts between the two regions show that gust fronts that propagate downhill into and along the Rio Grande Valley in NM are generally associated with faster propagation speeds ($\overline{pspd} = 8.6\,m\,s^{-1}$), larger decreases in temperature ($\Delta\overline{T} = -2.2$°C), and larger increases in horizontal wind speeds ($\Delta\overline{wsp} = 7.5\,m\,s^{-1}$) and wind direction ($\Delta\overline{wdir} = 76.5$°) compared to gust fronts that reach the crest of the Mogollon Rim in AZ ($\overline{pspd} = 5.2\,m\,s^{-1}$; $\Delta\overline{T} = -1.5$°C; $\Delta\overline{wsp} = 3.5\,m\,s^{-1}$; $\Delta\overline{wdir} = 53.1$°). The results suggest that gust fronts that primarily propagate downhill into (between −3° and −22°) and within a valley may induce larger increases in wind speed during passage compared to those that

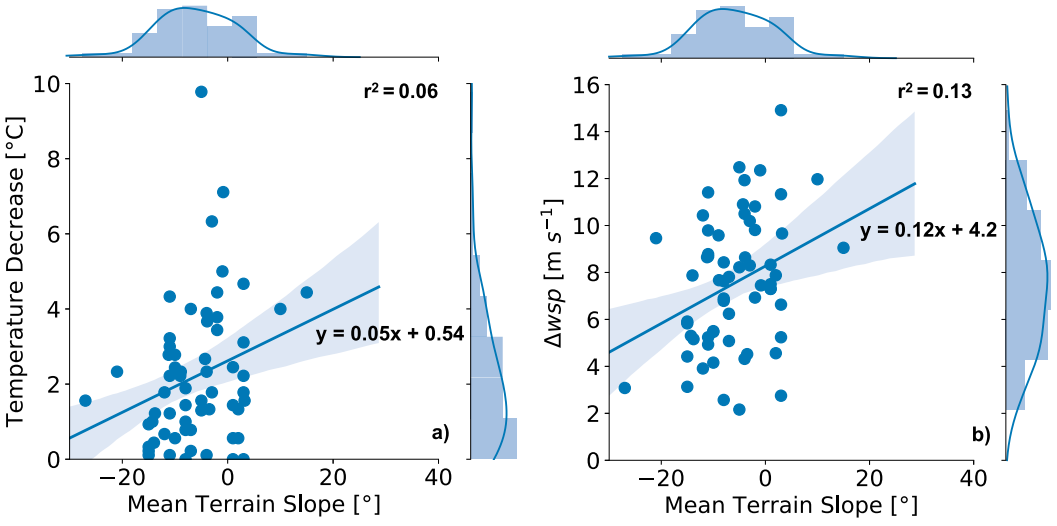

FIG. 12. As in Fig. 9, but comparison of (a) the decrease in temperature (°C), and (b) the magnitude change in wind speed ($m\,s^{-1}$) measured by the New Mexico KABQ ASOS station, each as a function of the mean directional terrain slope (°) calculated along the propagation path for each individual gust front.

are pushed uphill (between 20° and 27°) to or propagate atop a ridgeline. These findings agree with Kishcha et al. (2016) who also observed strong maximum horizontal wind speeds ($\Delta\widetilde{wsp} = 12\,m\,s^{-1}$) associated with a downslope-accelerated gust front on the lee side of the Judean Mountains in the Dead Sea valley. Conversely, Luchetti et al. (2020) observed $\Delta\widetilde{wsp}$ increases of $<4\,m\,s^{-1}$ close to the surface (<25 m AGL) across 24 gust fronts that primarily propagated uphill to study sites located in the Colorado Front Range. These values are similar to those produced by the AZ gust fronts studied atop the Mogollon Rim ($2.9 < \Delta\widetilde{wsp} < 4.8\,m\,s^{-1}$), but weaker than the gust fronts that propagated downhill into and along the Rio Grande Valley in NM ($5.2 < \Delta\widetilde{wsp} < 8.7\,m\,s^{-1}$). Therefore, the results in this study support observational findings from previous work suggesting that gust fronts that travel downslope (upslope) can accelerate (decelerate) and induce larger (smaller) increases in wind speed (Kishcha et al. 2016; Luchetti et al. 2020). Furthermore, laboratory and numerical experiments of density current interactions with upslope inclines show that as the upslope angle increases, density currents become thinner and gravity parallel to the upslope induces a deceleration of the density current (Marleau et al. 2014; Lombardi et al. 2015; De Falco et al. 2020). For density currents propagating downslope, an acceleration phase is observed as available potential energy

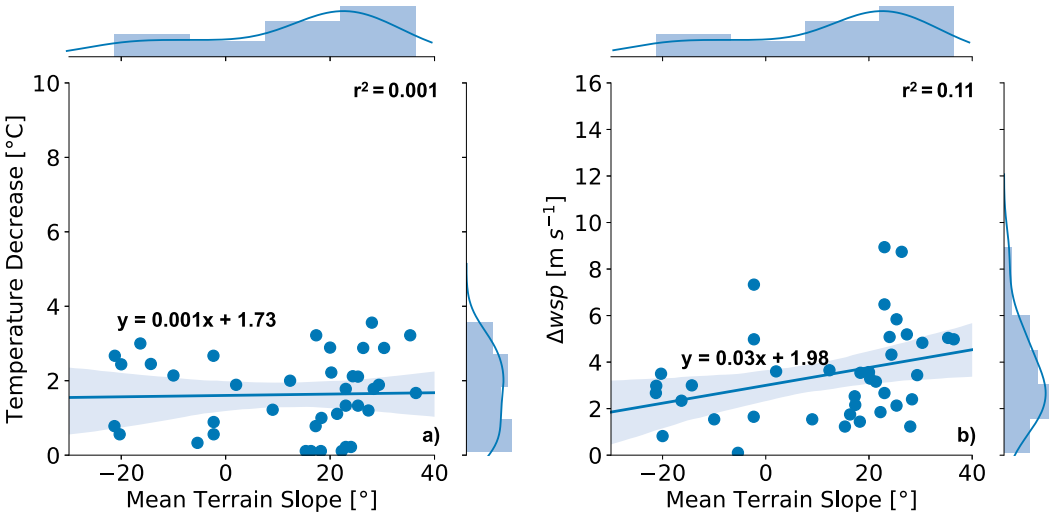

FIG. 13. As in Fig. 9, but comparison of (a) the decrease in temperature (°C), and (b) the magnitude change in wind speed ($m\,s^{-1}$) measured by the Arizona KFLG ASOS station, each as a function of the mean directional terrain slope (°) calculated along the propagation path for each individual gust front.

is converted into kinetic energy (Dai et al. 2012; Dai and Huang 2016; He et al. 2017). Since gust fronts often behave like density currents (Charba 1974; Sasaki and Baxter 1986; Friedrich et al. 2005), differences in propagation speed between gust fronts pushed up to and atop the Mogollon Rim in AZ ($\overline{\text{pspd}} = 5.2\,\text{m s}^{-1}$) and those that propagate downhill into and along the Rio Grande Valley in NM ($\overline{\text{pspd}} = 8.6\,\text{m s}^{-1}$) provides observational evidence supporting the results of previous laboratory experiments investigating the influence of upslope and downslope surfaces on density current speed.

5. Conclusions

This study quantifies the variability in propagation speed and atmospheric characteristics across 122 gust fronts that occur in the complex terrain of NM and AZ during the 2010–18 monsoon seasons (June–August). Using radar and ASOS station data, gust fronts that were pushed uphill and propagated atop the crest of the Mogollon Rim in AZ were compared to those that propagated down into or along the Rio Grande Valley in NM to assess how variability in terrain may influence gust front characteristics. The main findings from this analysis are as follows:

- Gust fronts that propagated downhill into and along the Rio Grande Valley in NM were generally associated with faster propagation speeds ($\overline{\text{pspd}} = 8.6\,\text{m s}^{-1}$), slightly larger decreases in temperature ($\Delta\overline{T} = -2.2°\text{C}$), larger increases in horizontal wind speeds ($\Delta\overline{\text{wsp}} = 7.5\,\text{m s}^{-1}$), and changes in wind direction ($\Delta\overline{\text{wdir}} = 76.5°$) compared to gust fronts that reached the crest of the Mogollon Rim in AZ ($\overline{\text{pspd}} = 5.2\,\text{m s}^{-1}$; $\Delta\overline{T} = -1.5°\text{C}$; $\Delta\overline{\text{wsp}} = 3.5\,\text{m s}^{-1}$; $\Delta\overline{\text{wdir}} = 53.1°$).
- The prefrontal ambient wind was not a strong determining factor for gust front propagation speed ($r = 0.26$; $R^2 = 0.07$) for those that propagated downhill into and along the Rio Grande Valley in NM. However, faster (slower) AZ gust fronts often did have stronger tailwinds (headwinds) ($r = 0.57$; $R^2 = 0.32$), and thus the prefrontal ambient wind did moderately influence propagation speed for the cases studied atop the Mogollon Rim in AZ.
- Gust fronts that propagated downhill into the Rio Grande Valley in NM behaved more in accordance with traditional density current theory than those that were pushed uphill and propagated atop the Mogollon Rim in AZ. In the theory, the stronger the difference in temperature between the boundary and the ambient air, the stronger the wind speeds behind the two air masses. Here, the relationship between the magnitude decrease in temperature and magnitude increase in wind speed was stronger for gust fronts that propagated down into and along the Rio Grande Valley in NM ($r = 0.57$; $R^2 = 0.33$) compared to those atop the Mogollon Rim in AZ ($r = 0.28$, $R^2 = 0.08$).
- For gust fronts that propagated downhill and within the Rio Grande Valley in NM, larger magnitude decreases in temperature were weakly associated with those that encountered less negative mean terrain slopes ($r = 0.24$; $R^2 = 0.06$). Similarly, larger magnitude changes in wind speed were also associated with less negative mean terrain slopes ($r = 0.36$; $R^2 = 0.13$). For gust fronts that propagated uphill and atop the Mogollon Rim in AZ, no discernable relationships between upslope or downslope adiabatic processes and gust front wind speed and temperature drop was found.

Results from this study provide an initial step in understanding the influence of common terrain features on propagating thunderstorm gust fronts. A future study should compare the results here to other terrain regions where gust fronts either propagate down into valleys or get pushed up and over ridgelines, or to those that interact with other terrain features such as plateaus or depressions. Additional observations could benefit numerical models that must be able to accurately incorporate the influence of terrain features on the strength and modification of thunderstorm gust fronts. This is particularly true for operational turbulence-resolving fire models, where their accuracy is highly dependent on the model's ability to simulate realistic turbulent boundaries in the vicinity of wildfires in areas of complex terrain.

One potential limitation here, however, is that we are trying to link gust front characteristics observed at a fixed location in time and space to the mean slope across the entire terrain profile. While the mean slope may suggest a primarily downhill path, for example, the actual profile likely includes alternating uphill and downhill sections (e.g., West Central Highlands in Fig. 5). Therefore, a future study could utilize a Lagrangian modeling approach to quantify the changes in gust front characteristics at every uphill and downhill stretch of the profile. This type of approach would likely yield a better understanding of whether or not downslope or upslope adiabatic processes influence gust front characteristics.

Acknowledgments. This research is supported through an Award L17AC00227 (''JFSP Project 17-1-05-2 Evaluating thunderstorm outflow boundaries in WRF-Fire'') from the Bureau of Land Management (BLM) as part of the Joint Fire Science Program under the subject opportunity FA-FON0017-0002. The authors thank Craig Schwartz of NCAR and the anonymous reviewer of this manuscript for their comments and suggestions, which strengthened the fundamentals of this article.

Data availability statement. All radar and ASOS data used for this analysis are openly available from the NOAA National Centers for Environmental Information (NCEI) data archives. Radar data are available at https://www.ncdc.noaa.gov/nexradinv/. All ASOS station data are available at https://www.ncdc.noaa.gov/data-access/land-based-station-data/land-based-datasets/automated-surface-observing-system-asos.

REFERENCES

Adams, D. K., and A. C. Comrie, 1997: The North American monsoon. *Bull. Amer. Meteor. Soc.*, **78**, 2197–2214, https://doi.org/10.1175/1520-0477(1997)078<2197:TNAM>2.0.CO;2.

Arritt, R. W., 1993: Effects of the large-scale flow on characteristic features of the sea breeze. *J. Appl. Meteor.*, **32**, 116–125, https://doi.org/10.1175/1520-0450(1993)032<0116:EOTLSF>2.0.CO;2.

Ashley, W. S., A. M. Haberlie, and J. Strohm, 2019: A climatology of quasi-linear convective systems and their hazards in the

United States. *Wea. Forecasting*, **34**, 1605–1631, https://doi.org/10.1175/WAF-D-19-0014.1.

Benjamin, T. B., 1968: Gravity currents and related phenomena. *J. Fluid Mech.*, **31**, 209–248, https://doi.org/10.1017/S0022112068000133.

Bosart, L. F., A. Seimon, K. D. LaPenta, and M. J. Dickinson, 2006: Supercell tornadogenesis over complex terrain: The Great Barrington, Massachusetts, tornado on 29 May 1995. *Wea. Forecasting*, **21**, 897–922, https://doi.org/10.1175/WAF957.1.

Bryan, G. H., and M. D. Parker, 2010: Observations of a squall line and its near environment using high-frequency rawinsonde launches during VORTEX2. *Mon. Wea. Rev.*, **138**, 4076–4097, https://doi.org/10.1175/2010MWR3359.1.

Bunkers, M. J., M. R. Hjelmfelt, and P. L. Smith, 2006: An observational examination of long-lived supercells. Part I: Characteristics, evolution, and demise. *Wea. Forecasting*, **21**, 673–688, https://doi.org/10.1175/WAF949.1.

Charba, J., 1974: Application of gravity current model to analysis of squall-line gust front. *Mon. Wea. Rev.*, **102**, 140–156, https://doi.org/10.1175/1520-0493(1974)102<0140:AOGCMT>2.0.CO;2.

Coen, J. L., and W. Schroeder, 2017: Coupled weather-fire modeling: From research to operational forecasting. *Fire Manage. Today*, **75**, 39–45.

——, E. N. Stavros, and J. A. Fites-Kaufman, 2018: Deconstructing the King megafire. *Ecol. Appl.*, **28**, 1565–1580, https://doi.org/10.1002/eap.1752.

Cotton, W. R., R. L. George, P. J. Wetzel, and R. L. McAnelly, 1983: A long-lived mesoscale convective complex. Part I: The mountain-generated component. *Mon. Wea. Rev.*, **111**, 1893–1918, https://doi.org/10.1175/1520-0493(1983)111<1893:ALLMCC>2.0.CO;2.

Dai, A., and Y. L. Huang, 2016: High-resolution simulations of non-Boussinesq downslope gravity currents in the acceleration phase. *Phys. Fluids*, **28**, 026602, https://doi.org/10.1063/1.4942239.

——, C. E. Ozdemir, M. I. Cantero, and S. Balachandar, 2012: Gravity currents from instantaneous sources down a slope. *J. Hydraul. Eng.*, **138**, 237–246, https://doi.org/10.1061/(ASCE)HY.1943-7900.0000500.

De Falco, M. C., L. Ottolenghi, and C. Adduce, 2020: Dynamics of gravity currents flowing up a slope and implications for entrainment. *J. Hydraul. Eng.*, **146**, 04020011, https://doi.org/10.1061/(ASCE)HY.1943-7900.0001709.

Droegemeier, K. K., and R. B. Wilhelmson, 1987: Numerical simulation of thunderstorm outflow dynamics. Part I: Outflow sensitivity experiments and turbulence dynamics. *J. Atmos. Sci.*, **44**, 1180–1210, https://doi.org/10.1175/1520-0469(1987)044<1180:NSOTOD>2.0.CO;2.

Engerer, N. A., D. J. Stensrud, and M. C. Coniglio, 2008: Surface characteristics of observed cold pools. *Mon. Wea. Rev.*, **136**, 4839–4849, https://doi.org/10.1175/2008MWR2528.1.

ESRI, 2011: ArcGIS Desktop: Release 10. Environmental Systems Research Institute.

Friedrich, K., D. E. Kingsmill, and C. R. Young, 2005: Misocyclone characteristics along Florida gust fronts during CaPE. *Mon. Wea. Rev.*, **133**, 3345–3367, https://doi.org/10.1175/MWR3040.1.

Fujita, T. T., 1981: Tornadoes and downbursts in the context of generalized planetary scales. *J. Atmos. Sci.*, **38**, 1511–1534, https://doi.org/10.1175/1520-0469(1981)038<1511:TADITC>2.0.CO;2.

Gilliam, R. C., S. Raman, and D. D. S. Niyogi, 2004: Observational and numerical study on the influence of large-scale flow direction and coastline shape on sea-breeze evolution. *Bound.-Layer Meteor.*, **111**, 275–300, https://doi.org/10.1023/B:BOUN.0000016494.99539.5a.

Goens, D. W., and P. L. Andrews, 1998: Weather and fire behavior factors related to the 1990 Dude Fire near Payson, AZ. *Second Conf. on Fire and Forest Meteorology*, Phoenix, AZ, Amer. Meteor. Soc., 153–158.

Goff, R. C., 1976: Vertical structure of thunderstorm outflows. *Mon. Wea. Rev.*, **104**, 1429–1440, https://doi.org/10.1175/1520-0493(1976)104<1429:VSOTO>2.0.CO;2.

Haines, D. A., 1988: Downbursts and wildland fires: A dangerous combination. *Fire Manage. Today*, **49**, 8–10.

Hanley, D. E., P. Cunningham, and S. L. Goodrick, 2013: Interaction between a wildfire and the sea-breeze front. *Remote Sensing and Modeling Applications to Wildland Fires*, J. J. Qu et al., Eds., Springer, 81–98, https://doi.org/10.1007/978-3-642-32530-4_7.

Hardy, K., and L. K. Comfort, 2015: Dynamic decision processes in complex, high-risk operations: The Yarnell Hill Fire, June 30, 2013. *Saf. Sci.*, **71**, 39–47, https://doi.org/10.1016/j.ssci.2014.04.019.

He, Z., L. Zhao, T. Lin, P. Hu, Y. Iv, H.-C. Ho, and Y.-T. Lin, 2017: Hydrodynamics of gravity currents down a ramp in linearly stratified environments. *J. Hydraul. Eng.*, **143**, 04016085, https://doi.org/10.1061/(ASCE)HY.1943-7900.0001242.

Johnson, R. H., R. S. Schumacher, J. H. Ruppert, D. T. Lindsey, J. E. Ruthford, and L. Kriederman, 2014: The role of convective outflow in the Waldo Canyon Fire. *Mon. Wea. Rev.*, **142**, 3061–3080, https://doi.org/10.1175/MWR-D-13-00361.1.

Joint Fire Science Program, 2017: Validating mesoscale, atmospheric boundary prediction models and tools. Project Announcement FA-FON0017-0001, 25 pp., https://www.firescience.gov/AFPs/17-1-05/17-1-05_FON_Announcement.pdf.

Jorgensen, D. P., Z. Pu, P. O. Persson, and W. Tao, 2003: Variations associated with cores and gaps of a Pacific narrow cold frontal rainband. *Mon. Wea. Rev.*, **131**, 2705–2729, https://doi.org/10.1175/1520-0493(2003)131<2705:VAWCAG>2.0.CO;2.

Karels, J., and M. Dudley, 2013: Yarnell Hill Fire serious accident investigation report. Arizona State Forestry Division, 116 pp., https://sites.google.com/site/yarnellreport/.

Keighton, S., J. Jackson, J. Guyer, and J. Peters, 2007: A preliminary analysis of severe quasilinear mesoscale convective systems crossing the Appalachians. *22nd Conf. on Weather Analysis and Forecasting/18th Conf. on Numerical Weather Prediction*, Park City, UT, Amer. Meteor. Soc., P2.18, https://ams.confex.com/ams/pdfpapers/123614.pdf.

Kern, J., W. Jones, J. Murrian, and J. DiMaggio, 2004: Review of burnover incident at St Sebastian River Preserve State Park, Indian River County, Florida, 24 February 2004. Florida Department of Environmental Protection, 25 pp.

Kishcha, P., and Coauthors, 2016: Modelling of a strong dust event in the complex terrain of the Dead Sea valley during the passage of a gust front. *Tellus*, **68B**, 29751, https://doi.org/10.3402/tellusb.v68.29751.

Koch, S. E., and C. A. Ray, 1997: Mesoanalysis of summertime convergence zones in central and eastern North Carolina. *Wea. Forecasting*, **12**, 56–77, https://doi.org/10.1175/1520-0434(1997)012<0056:MOSCZI>2.0.CO;2.

LaPenta, K. D., L. F. Bosart, T. J. Galarneau, and M. J. Dickinson, 2005: A multiscale examination of the 31 May 1998 Mechanicville, New York, tornado. *Wea. Forecasting*, **20**, 494–516, https://doi.org/10.1175/WAF875.1.

Lombardi, V., C. Adduce, G. Sciortino, and M. La Rocca, 2015: Gravity currents flowing upslope: Laboratory experiments and shallow-water simulations. *Phys. Fluids*, **27**, 016602, https://doi.org/10.1063/1.4905305.

Lompar, M., M. Ćurić, and D. Romanic, 2018: Implementation of a gust front head collapse scheme in the WRF numerical model. *Atmos. Res.*, **203**, 231–245, https://doi.org/10.1016/j.atmosres.2017.12.018.

Luchetti, N. T., K. Friedrich, C. E. Rodell, and J. K. Lundquist, 2020: Characterizing thunderstorm gust fronts near complex terrain. *Mon. Wea. Rev.*, **148**, 3267–3286, https://doi.org/10.1175/MWR-D-19-0316.1.

Marleau, L. J., M. R. Flynn, and B. R. Sutherland, 2014: Gravity currents propagating up a slope. *Phys. Fluids*, **26**, 046605, https://doi.org/10.1063/1.4872222.

McAnelly, R. L., and W. R. Cotton, 1986: Meso-β-scale characteristics of an episode of meso-α-scale convective complexes. *Mon. Wea. Rev.*, **114**, 1740–1770, https://doi.org/10.1175/1520-0493(1986)114<1740:MSCOAE>2.0.CO;2.

Nadolski, V., 1998: Automated Surface Observing System (ASOS) user's guide. National Oceanic and Atmospheric Administration, Department of Defense, Federal Aviation Administration, U.S. Navy, 74 pp., https://www.weather.gov/media/asos/aum-toc.pdf.

NWS, 2008: Cup & vane wind data processing within ASOS. NWS, 2 pp., https://www.weather.gov/media/asos/ASOS%20Implementation/IFWS_BelfordWS_comparison.pdf.

Paez, G., M. Strojnik, and M. K. Scholl, 2015: Analysis of propagation of complex fire: Case of the Yarnell Hill Fire 1. *Proc. SPIE*, **9608**, 96081L, https://doi.org/10.1117/12.2191725.

Parker, M. D., and D. A. Ahijevych, 2007: Convective episodes in the east-central United States. *Mon. Wea. Rev.*, **135**, 3707–3727, https://doi.org/10.1175/2007MWR2098.1.

Sasaki, Y. K., and T. L. Baxter, 1986: The gust front. *Thunderstorm Morphology and Dynamics*, E. Kessler, Ed., University of Oklahoma, 187–196.

Schneider, D. G., 2009: The impact of terrain on three cases of tornadogenesis in the Great Tennessee Valley. *Electron. J. Oper. Meteor.*, **EJ11**, 1–33, https://nwafiles.nwas.org/ej/pdf/2009-EJ11.pdf.

Sharples, J. J., R. H. D. McRae, C. Simpson, P. Fox-Hughes, and C. Clements, 2017: Terrain-controlled airflows. *Fire Manage. Today*, **75**, 20–24.

Shipley, S. T., A. Peterlin, and S. Cantrell, 2009: Radar visualization and occultation in 4-dimensions using Google Earth. *25th Conf. on IIPS*, Phoenix, AZ, Amer Meteor. Soc., 12.1, https://ams.confex.com/ams/pdfpapers/150724.pdf.

Simpson, J. E., 1969: A comparison between laboratory and atmospheric density currents. *Quart. J. Roy. Meteor. Soc.*, **95**, 758–765, https://doi.org/10.1002/qj.49709540609.

——, and R. E. Britter, 1980: A laboratory model of an atmospheric mesofront. *Quart. J. Roy. Meteor. Soc.*, **106**, 485–500, https://doi.org/10.1002/qj.49710644907.

Smith, B. T., R. L. Thompson, J. S. Grams, C. Broyles, and H. E. Brooks, 2012: Convective modes for significant severe thunderstorms in the contiguous United States. Part I: Storm classification and climatology. *Wea. Forecasting*, **27**, 1114–1135, https://doi.org/10.1175/WAF-D-11-00115.1.

Surveys and Investigation Staff, 1981: A report to the committee on appropriations U.S. House of Representatives on wildfire on Merritt Island. December 1981, 34 pp., https://www.wildfirelessons.net/HigherLogic/System/DownloadDocumentFile.ashx?DocumentFileKey=de70dc82-1760-487f-b1d4-05a8d11293cc&forceDialog=0.

Tucker, D. F., and N. A. Crook, 1999: The generation of a mesoscale convective system from mountain convection. *Mon. Wea. Rev.*, **127**, 1259–1273, https://doi.org/10.1175/1520-0493(1999)127<1259:TGOAMC>2.0.CO;2.

Wakimoto, R. M., C. J. Kessinger, and D. E. Kingsmill, 1994: Kinematic, thermodynamic, and visual structure of low-reflectivity microbursts. *Mon. Wea. Rev.*, **122**, 72–92, https://doi.org/10.1175/1520-0493(1994)122<0072:KTAVSO>2.0.CO;2.

Wilson, J. W., and W. E. Schreiber, 1986: Initiation of convective storms at radar-observed boundary-layer convergence lines. *Mon. Wea. Rev.*, **114**, 2516–2536, https://doi.org/10.1175/1520-0493(1986)114<2516:IOCSAR>2.0.CO;2.